Electronic properties and charge transfer phenomena in Pt nanoparticles on γ-Al₂O₃: size, shape, support, and adsorbate effects†

F. Behafarid,[a] L. K. Ono,[a] S. Mostafa,[a] J. R. Croy,[a] G. Shafai,[a] S. Hong,[a] T. S. Rahman,*[a] Simon R. Bare[b] and B. Roldan Cuenya*[a]

This study presents a systematic detailed experimental and theoretical investigation of the electronic properties of size-controlled free and γ-Al₂O₃-supported Pt nanoparticles (NPs) and their evolution with decreasing NP size and adsorbate (H_2) coverage. A combination of *in situ* X-ray absorption near-edge structure (XANES) and density functional theory (DFT) calculations revealed changes in the electronic characteristics of the NPs due to size, shape, NP–adsorbate (H_2) and NP–support interactions. A correlation between the NP size, number of surface atoms and coordination of such atoms, and the maximum hydrogen coverage stabilized at a given temperature is established, with H/Pt ratios exceeding the 1 : 1 ratio previously reported for bulk Pt surfaces.

1. Introduction

Striking changes in the physical and chemical properties of small metal nanoparticles (NPs) have been reported,[1–7] and in some cases assigned to size-dependent modifications of their electronic properties, including metal/non-metal transitions, the discretization of energy levels, and rehybridization of spd orbitals.[2,8] Nevertheless, in addition to intrinsic changes in the NP properties brought about by specific geometrical features (*e.g.* NP size and shape), the role of external influences such as adsorbate and support effects must also be taken into consideration.

Although significant effort has been dedicated to the investigation of geometric and environmental effects on the electronic properties of metal NPs,[9–17] some discrepancies still remain in the literature regarding the interpretation of certain experimental trends.[16,18–21] These are due in part to the challenge of synthesizing geometrically well-defined target material systems, the difficulty of separating the different influences on a given electronic property (since some correlations exist among them), and the complexity of real-world experimental NP supports, making related modeling descriptions difficult.

In situ X-ray absorption near edge structure (XANES) measurements have proven valuable for the study of intrinsic and extrinsic effects on the electronic properties of NPs,[9–16,19,22–27] since this technique is sensitive to unoccupied electronic states. The following differences have been observed when comparing XANES data of nanoscale systems to bulk systems: (i) modifications in the intensity of the absorption edge peak (or white line, WL), (ii) an increase/decrease in the width of the WL, and (iii) a shift in the energy of the absorption edge. The extent of these modifications was found to be strongly influenced by extrinsic effects. More specifically, changes in L_3 and L_2 XANES spectra of metals upon chemisorption can be explained in terms of orbital hybridization, charge transfer, and metal–adsorbate scattering.

Although general agreement exists on the correlation between the integrated area of the adsorption peak and the amount of chemisorbed hydrogen,[16,18–21] it is still unclear whether the peak energy is influenced by the number of H adsorption sites on the NP surface, the presence of co-adsorbates, and the NP size/shape. In the absence of adsorbed hydrogen, a narrowing of the electron density of states (DOS) and a shift of the d-band center towards E_F have been theoretically described by comparing unsupported Pt_6 NPs and Pt(111), highlighting that intrinsic effects must also be considered.[16]

In addition to adsorbate effects, the interaction of the NPs with the underlying support must also be addressed. This is, however, a difficult task, since due to specifics of the most common NP synthesis approaches used, a direct comparison of the influence of different supports on NPs of identical geometry (same size and shape) cannot normally be conducted, leading to a convolution of support (extrinsic) and size/shape (intrinsic) effects. Some groups report a lack of correlation between the intensity of the absorption peak, integrated area or energy, and the type of NP support,[22,23,28] exclusively assigning the changes observed to adsorbate chemisorption. On the other hand, a theoretical study of a Pt_6 cluster in a zeolite-LTL pore revealed a broadening of the WL for the supported cluster with respect to bare Pt_6 and a concomitant decrease in the WL intensity in order to maintain the overall

[a] *Department of Physics, University of Central Florida, Orlando, Florida 32816, USA. E-mail: roldan@ucf.edu, talat.rahman@ucf.edu*
[b] *UOP LLC, a Honeywell Company, Des Plaines, IL 60017, USA*
† Electronic supplementary information (ESI) available. See DOI: 10.1039/c2cp41928a

density of d-states constant.[10] For Pt NPs on carbon nanotubes, the smaller WL of the NPs as compared to bulk Pt was assigned to charge redistribution between C-2p and Pt-5d states, which did not lead to the loss of charge.[12] For Pt NPs on SiO$_2$, the increase in the WL observed was assigned to charge transfer from Pt to SiO$_2$.[12] This is another controversial aspect in the literature, since some groups explain the observed changes in the XANES data (e.g. energy shift) based on charge transfer phenomena (to/from adsorbates or the support), while others on the formation of metal–adsorbate or metal–support bonds (charge redistribution) leading to changes in the electron density of states near the Fermi level.[19,29] Furthermore, theoretically predicted fluctuating cluster–substrate interactions and charge transfer phenomena for Pt$_{10}$ on γ-Al$_2$O$_3$ were correlated with the positive energy shifts experimentally observed with decreasing NP size and decreasing measurement temperature.[11]

The present study takes advantage of state-of-the-art nanostructure fabrication, characterization and *ab initio* modeling to gain deep insight into the role played by the geometrical structure of NPs (size and shape), support, and surface adsorbates, on their electronic properties. Specifically, we used size- and shape-selected Pt NPs (produced by micelle encapsulation methods) supported on γ-Al$_2$O$_3$ combined with synergistic *in situ* XANES, cluster shape modeling, and density functional theory (DFT). The ability of tuning the d-electron density in supported NPs *via* a rational geometrical design is key for the ultimate control of catalytic properties, since reactivity is strongly influenced by the interaction of d-orbitals of metals with valence orbitals of reactants.

2. Experimental and theoretical methods

(a) Sample preparation

Size- and shape-selected Pt NPs were prepared by micelle encapsulation methods. Poly(styrene)-block-poly(2vinylpyridine) [PS-P2VP] diblock copolymers were dissolved in toluene to form inverse micelles. Size-selected Pt NPs are created by dissolving H$_2$PtCl$_6$ into the polymeric solution. Subsequently, the nanocrystalline γ-Al$_2$O$_3$ support (Alfa Aesar, average crystalline size ∼40 nm) is added. The Pt loading is 1% by weight. The encapsulating ligands are eliminated by heating in 50% O$_2$ balanced by He at 648 K for 24 hours. Different NP sizes can be obtained by changing the molecular weight of the head (P2VP) of the encapsulating polymer, the metal–P2VP ratio (micelle loading), and the post-preparation annealing treatment and atmosphere.[30] Our micellar synthesis normally leads to 3D-like NP structures. Nevertheless, the NP shape can be changed from 3D to 2D by decreasing the metal loading into the initially spherical polymeric micelles. Further details on the sample preparation, synthesis parameters, and transmission electron microscopy (TEM) characterization can be found in ref. 30–35 and in Table 1.

(b) Structural, electronic characterization (XAFS), and nanoparticle shape modeling

Pt-L$_3$ edge X-ray absorption fine-structure spectroscopy (XAFS) data were acquired at beamline X18B of the NSLS
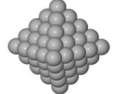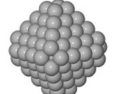
at Brookhaven National Laboratory in transmission mode. The XAFS samples were prepared by pressing the Pt/γ-Al$_2$O$_3$ powders into thin pellets which were mounted in a cell described previously,[36,37] that permitted sample heating *via* an external PID controller, liquid nitrogen cooling, as well as the continuous flow of gases during data acquisition. A Kapton window in the cell allows both *in situ* X-ray transmission and fluorescence measurements. A Pt foil was measured simultaneously with all samples for energy alignment and calibration purposes. Multiple scans were collected at each temperature of interest and averaged in order to improve the signal-to-noise ratio. Measurements were made at different temperatures under H$_2$ (50% H$_2$ balanced with He for a total flow rate of 50 ml min^{-1}, S1–S9) and He (S2) atmospheres. The sample measured in He was first reduced in H$_2$ at 648 K. Subsequently, the H$_2$ environment was replaced by He and XAFS data were acquired at different temperatures during cooling from 648 K to 173 K.

Quantitative determination of the average NP shape was carried out by analyzing low temperature (166–188 K) extended X-ray absorption fine structure spectroscopy (EXAFS) data up to the 4th nearest neighbor contribution, including multiple scattering paths as described in ref. 30, 33 and 35 and references therein. The *r* fitting range was 1.8 Å to 5.7 Å. The shapes of our Pt NPs have been resolved by matching structural information obtained experimentally *via* EXAFS (coordination numbers up to the 4th nearest neighbor, N$_1$–N$_4$) and TEM (NP diameter, *d*) to analogous data extracted from a self-generated database containing ∼4000 model fcc NP shapes.[30,38,39] Detailed structural characterization of the present samples is given in ref. 30, 38 and 39. Additional information on the determination of the NP shapes is included in the ESI.† Table 1 shows the shapes that best fitted the EXAFS and TEM data for each of the samples investigated and contains information on the ratio of the number of Pt atoms at the NP surface and perimeter to the total number of atoms within each NP (N$_s$/N$_t$) and that of the number of Pt atoms in contact with the support to the total number of atoms within a NP (N$_c$/N$_t$) extracted from the selected model NP shapes. As it is described in more detail in ref. 39, for each of the samples containing small Pt NPs, only 2–3 similar shapes were in good agreement with the EXAFS coordination numbers and TEM diameter (including the experimental error margins). No shapes are displayed in this manuscript for the samples containing large NPs (S7–S9), since a large number of cluster shapes are in agreement with the EXAFS coordination numbers and TEM diameters.[40]

Changes in the morphology of our samples as a function of temperature have not been accounted for in our analysis since our EXAFS measurements were conducted up to a maximum temperature of 648 K, which is the same temperature used for sample calcination (24 h) prior to the *in situ* spectroscopy analysis. If any changes in the NP morphology (size and/or shape) were to occur at 648 K, they should have already taken place before the XAFS measurements.

In order to gain insight into the electronic properties of Pt NPs, we present here XANES spectra from the Pt-L$_3$ absorption edge. These data provide information on the binding energies of 2p electrons (2p$_{3/2}$ initial state) and the unoccupied "d"

This journal is © the Owner Societies 2012

Phys. Chem. Chem. Phys., 2012, **14**, 11766–11779 | 11767

Table 1 Parameters used for the synthesis of micellar Pt NPs, including polymer type (PS-PVP) and the ratio (L) between the metal salt loading and the molecular weight of the polymer head (P2VP). Also included are the mean TEM diameters from ref. 38. By comparing structural information obtained *via* EXAFS (1st–4th nearest neighbor coordination numbers) and TEM (NP diameters) with a database containing fcc-cluster shapes, the ratio of the number of surface atoms to the total number of atoms in a NP (N_s/N_t) and the ratio of the number of atoms in contact with the substrate to the total number of atoms (N_c/N_t) were obtained (see details in ref. 38). The NP shapes obtained for large NPs in S7–S9 are not shown in this table due to the large shape degeneracy for the obtained coordination number and TEM diameter

Sample name	Polymer	L	TEM diameter (nm)	Model cluster shapes	N_t	N_s/N_t	N_c/N_t
S1	PS(27700)-P2VP(4300)	0.06	0.8 ± 0.2		22	0.86	0.55
S2	PS(27700)-P2VP(4300)	0.1	0.8 ± 0.2		44	0.84	0.23
S3	PS(27700)-P2VP(4300)	0.2	1.0 ± 0.2		85	0.74	0.18
S4	PS(16000)-P2VP(3500)	0.05	1.0 ± 0.2		33	0.82	0.55
S5	PS(16000)-P2VP(3500)	0.1	1.0 ± 0.2		55	0.75	0.16
S6	PS(16000)-P2VP(3500)	0.2	1.0 ± 0.2		140	0.64	0.13
S7	PS(16000)-P2VP(3500)	0.4	1.8 ± 1.5				
S8	PS(27700)-P2VP(4300)	0.3	3.3 ± 1.5				
S9	PS(27700)-P2VP(4300)	0.6	5.4 ± 3.0				

electron density of states near the Fermi level ($d_{5/2}$ + $d_{3/2}$ states). Since the intensity and integrated area of the Pt-L_3 absorption peak are considered to be proportional to the density of unoccupied 5d electronic states, they can be used to extract information on d-level electronic charge redistributions.[41] It should be noted that our experimental set-up, along with our calibration procedures, allows us to discern relative energy shifts in the XANES peak position with sensitivity of about 0.1 eV. In order to obtain the peak position, the experimental data were fitted with a spline curve. In the following section, we will also provide information on the changes of the area of the Pt-L_3 absorption peak. Different methods have been used in the literature to calculate this area before and after NP/adsorbate exposure.[15,16,19,20,22,23,42–45] We have used the area of the second feature (called peak B) observed in raw (not artificially aligned) difference ΔXANES spectra as the representative parameter. In particular, ΔXANES areas were obtained by subtracting the XANES spectrum of the NPs at 648 K from that of the same sample measured at a given lower temperature, both in hydrogen. In the literature, some authors have shown similar ΔXANES plots using as reference spectra from a Pt foil,[16,23] or NPs measured under He[16,19,42] and vacuum.[15,20–23,25] Due to the inherent experimental difficulty of preventing the effect of trace oxygen and moisture possibly leading to the oxidization of small Pt NPs in conventional XAFS-compatible cells in the absence of H_2, we decided to use

as reference our highest temperature XANES spectra measured under H_2,[20] since a minimum H coverage on the NP surface is expected under those conditions, and lack of chemisorbed oxygen and/or NP oxidation is ensured under the continuous H_2 flow employed here. Additionally, total spectral areas were also obtained in the energy range between 11 564 and 11 580.6 eV after alignment of all NP spectra, Fig. S3(b) (ESI†).

(c) Theoretical methods

DFT calculations[46] were performed using the pseudopotential approximation and the projector augmented wave method, as implemented in the Vienna *Ab-Initio* Simulation Package (VASP).[47,48] The Kohn–Sham wave functions are expanded in the plane wave basis with a kinetic energy cutoff of 400 eV, and the Perdew–Burke–Ernzerhof functional used for the exchange–correlation energy.[49] Both unsupported bare Pt NPs (Pt_{22}, Pt_{33}, Pt_{44}, Pt_{55}, and Pt_{85}) and hydrogen-adsorbed Pt NPs ($Pt_{22}H_x$, x = 18, 22, 25, 27, 29, 31, 45, 59 and $Pt_{44}H_x$, x = 44, 60, 66) were investigated to provide insight into the experimental data. The H-adsorbed structures of $Pt_{22}H_x$ and $Pt_{44}H_x$ were prepared by first filling all low coordinated sites on the NPs with hydrogen atoms, followed by full ionic relaxation. Additional details of the model for the bare and hydrogen-adsorbed Pt NPs ($Pt_{22}H_x$, x = 22, 25, 27, 29, 31) can be found elsewhere.[38] The adsorption energy of a hydrogen

atom on a Pt NP was calculated by using $E_{ad} = (E[Pt_mH_x] - E[Pt_m] - x/2 \cdot E[H_2])/x$, where $E[]$ represents the DFT total energy of the NP of interest, and m and x are the number of Pt and H atoms in the NP, respectively. A supercell of dimension about $22 \times 22 \times 22$ Å^3 was used for the smaller NPs (Pt_{22}, Pt_{33}, Pt_{44}, Pt_{55}) and $27 \times 27 \times 27$ Å^3 for Pt_{85}. Because of the large size of the supercells used, only a single k-point was found to be sufficient for sampling the Brillouin zone. A Fermi-level smearing of 0.1 eV was used. The threshold for electronic energy convergence was set to 2×10^{-6} eV, and that for structural optimization to $<1 \times 10^2$ eV Å^{-1}. A standard quasi-Newtonian algorithm implemented in VASP was used for structural optimization. The angular-momentum-decomposed, local densities of states of the NPs were calculated by projecting the wave function into a sphere of radius of 1.45 Å centered at each Pt atom. Bader charge analysis[48,49] was performed to investigate charge transfer/redistribution upon H adsorption for Pt_{22} and Pt_{44} NPs.

3. Results

(a) Electronic properties (XANES)

The effects of the Pt NP size, shape, support, and chemical environment (adsorbates) on their electronic properties were investigated in situ via Pt-L$_3$ edge XANES. Fig. 1 shows the normalized absorption coefficient corresponding to the Pt-L$_3$ edge of Pt NPs with different sizes supported on γ-Al$_2$O$_3$ measured in H$_2$ at room temperature (RT) after in situ NP reduction at 648 K. The insets in Fig. 1(a) and (b) correspond to the model shapes that best represent the NPs in samples S1–S4. Two main differences were observed for the samples containing small NPs with respect to bulk Pt: (i) an increase in the width of the absorption peak, (ii) a shift in the absorption peak to higher energy.

The energy shift was found to be more significant for the NPs with 2D shape (S1, S4), Fig. 1(a). In particular, for samples containing NPs of identical average size (TEM diameter)[30,35,39] but different shape, the following energy shifts were measured: $\Delta E = +0.5$ eV for S1 with respect to S2 (0.8 ± 0.2 nm), and $+0.7$ eV for S4 with respect to S3 (1.0 ± 0.2 nm) (see Fig. S1 and S2, ESI†). Furthermore, for samples of identical shape (2D) but different size, e.g. 0.8 ± 0.2 nm NPs in S1 and 1.0 ± 0.2 nm in S4, Fig. 1(a), an increase in the width of the absorption peak was observed with decreasing NP size. The same was observed for the 3D NPs in Fig. 1(b). As expected, no drastic changes were observed in the XANES spectra of the samples containing large Pt NPs (S8, S9 > 3 nm) as compared to bulk Pt, Fig. 1(c).

In order to gain insight into the role of the adsorbate, the same sample S2 was measured in H$_2$ and He at low temperature (173 K). As can be seen in Fig. 1(d) in H$_2$, a broader absorption feature, higher WL intensity, and a larger energy shift with respect to the He data were observed. Complete saturation of the NP surface with H$_2$ is expected under these measurement conditions.
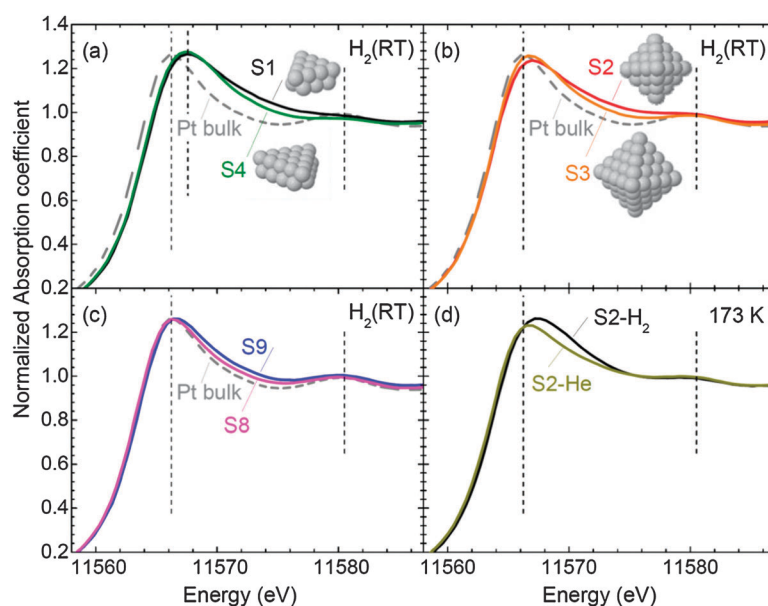
Fig. 2 displays temperature-dependent XANES data from Pt NPs with different sizes and shapes measured under an identical H$_2$ atmosphere: ~ 0.8 nm (S1, S2), ~ 1.0 nm (S3, S4), ~ 3.3 nm (S8), and ~ 5.4 nm (S9). The insets correspond to the model NP shapes extracted from the analysis of low-temperature (173–188 K) EXAFS data. Upon increasing the temperature from 173 K to 648 K, a decrease in the WL intensity, a shift towards lower energy, and a decrease in the linewidth were observed.

A linear correlation between both the energy shift of the absorption edge peak (with respect to bulk Pt) and its total area and the first nearest neighbor coordination number (N_1) was observed at RT: decreasing values with increasing N_1, Fig. 3(a) and (b), respectively. The blue shift of the WL observed for the NP samples relative to the Pt foil is most noticeable for S1 ($+1.35$ eV) but also present for the other samples ($+1.25$ eV for S4 and $+0.8$ for S2). A similar trend was observed when the former energy shifts are plotted versus the TEM NP diameter, Fig. 3(c), corroborating that the smallest NPs are the most affected by intrinsic (size and shape) as well as extrinsic (adsorbate and support) effects. It should be noted that the overall trend is the same if one uses the TEM diameter as a representative size parameter, Fig. 3(c), or the EXAFS NP size [e.g. 1st NN CN, Fig. 3(a)], although the dependence is slightly different, with a more abrupt change observed as a function of the NP diameter for NPs below ~ 1.5 nm. The difference is attributed to the fact that the EXAFS data (N_1) also contain structural information about the NP shape (not only its diameter), which, as will be discussed in more detail below, might play a role in the effect observed, via for example NP-support charge transfer for clusters with a large fraction of atoms in contact with the support. Analogous XANES data acquired at low-temperature (166 K–188 K) in H$_2$ are presented in Fig. S3 (ESI†).

In order to gain further insight into the role of adsorbed hydrogen in the electronic properties of our small fcc Pt NPs, ΔXANES plots were constructed. Fig. 4(a) displays XANES data from NPs with different sizes measured in H$_2$ at RT after subtraction of the 648 K spectrum of the respective NP sample. As was shown in our recent work,[38] significant H$_2$ desorption was predicted above 450 K (upon heating in an H$_2$ atmosphere), and therefore, it is reasonable to assume that the XANES data measured at 648 K are the ones least affected by chemisorbed hydrogen, and can therefore be used as reference of the state of the NPs with the minimum hydrogen coverage. Fig. 4(a) provides information on the hydrogen effect and effective hydrogen coverage on the surface of NPs of different sizes, with increasing spectral area with decreasing NP size. Quantitative analysis of these data will be shown later. Similar ΔXANES plots are included in Fig. 4(b) and (c), but in those cases the 648 K XANES spectra were subtracted from the data acquired in H$_2$ at different temperatures for samples S1 (b) and S9 (c) (the smallest and largest NPs). It should be noted that although the spectral features change drastically with temperature in the EXAFS region, XANES data are not strongly affected by thermal effects,[10] and therefore, comparisons such as the one described above are justified.

For the small NPs in S1, a clear trend of increasing spectral area with decreasing measurement temperature was detected, which correlates with the higher hydrogen coverage at the lowest measurement temperatures. As expected, due to the significantly lower surface to volume ratio of the NPs in S9, the adsorbate effect in Fig. 4(c) is small.

This journal is © the Owner Societies 2012

Phys. Chem. Chem. Phys., 2012, **14**, 11766–11779 | 11769

Fig. 1 Normalized absorption coefficient, $\mu(E)$, *versus* energy (XANES region) for the Pt-L$_3$ edge of Pt NPs on γ-Al$_2$O$_3$. The samples in (a–c) were measured at room temperature in H$_2$ after reduction (S1–S4). Similar data from a Pt foil are also displayed for reference. Sample S2 was measured in H$_2$ and He at 173 K (d).
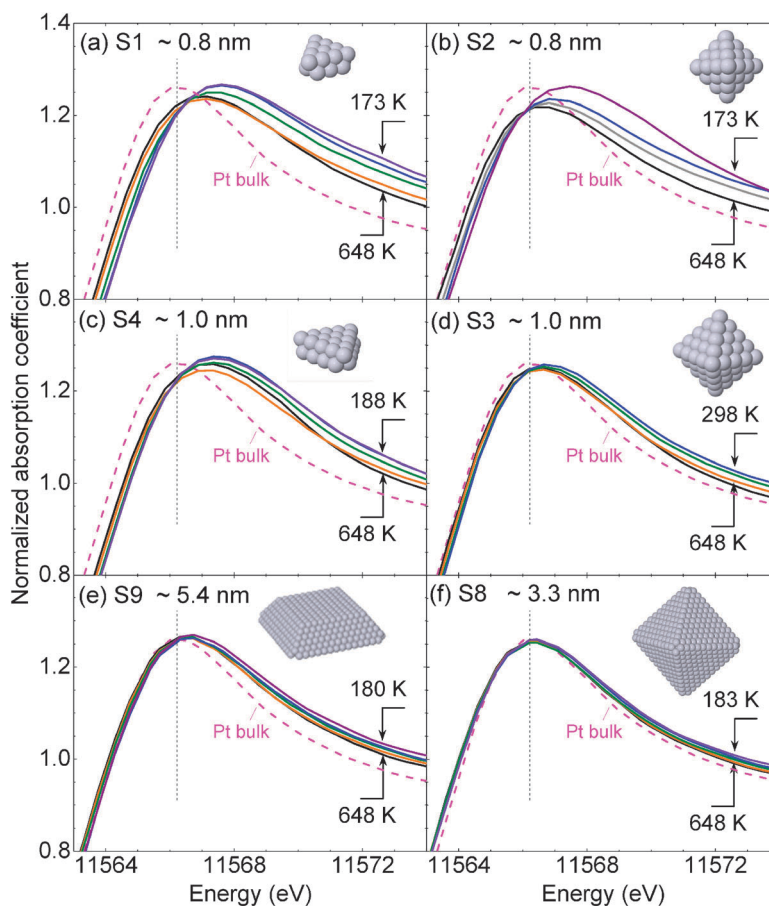
Fig. 2 Normalized absorption coefficient, $\mu(E)$, *versus* energy (XANES region) for the Pt-L$_3$ edge of Pt NPs on γ-Al$_2$O$_3$: (a) S1, (b) S2, (c) S4, (d) S3, (e) S9, (f) S8. Temperature dependent data acquired in H$_2$ from 173 K to 648 K are shown for all samples. The insets correspond to model NP shapes representative of the NPs in each of the samples. For the large NPs (S8 and S9), a large degeneracy of shapes was obtained, and the models shown in (e,f) are only a guide to the possible NP structures.
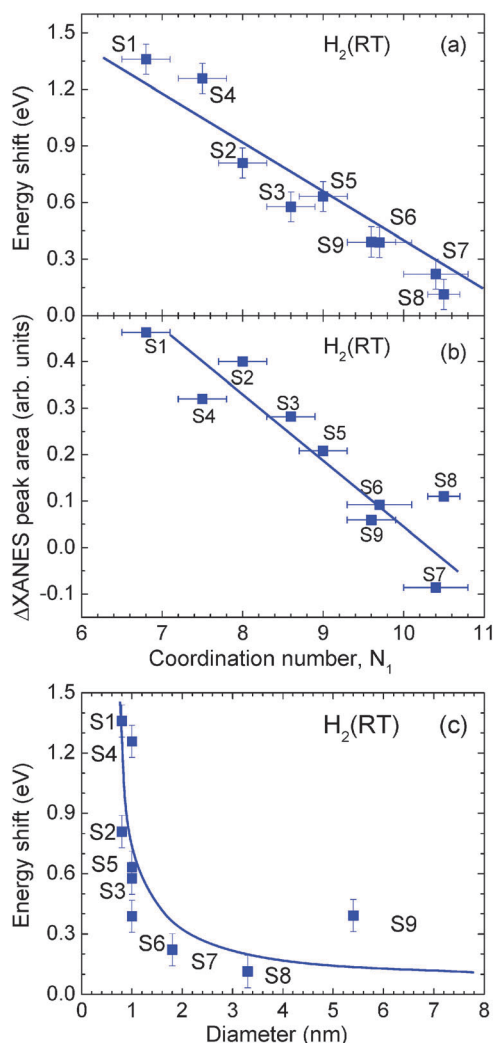
Fig. 3 Shift in the energy of the Pt-L_3 absorption edge of Pt NPs on γ-Al$_2$O$_3$ with respect to a bulk Pt reference as a function of: (a) the 1st nearest neighbor (NN) coordination number (CN), and (c) the TEM NP diameter from ref. 38. (b) Evolution of the ΔXANES area (peak B) of NPs with different sizes as a function of the 1st NN CN. The ΔXANES plots were obtained by subtracting XANES spectra measured under H$_2$ at 648 K (adsorbate-free) from those measured at RT under H$_2$ (nearly H-saturated).
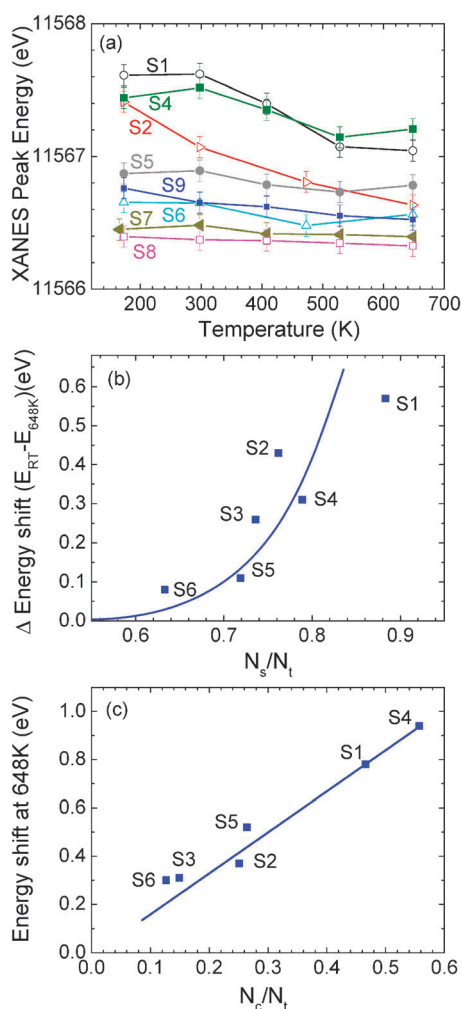
In order to evaluate the relative contribution of NP-adsorbate and NP-support charge transfer and redistribution phenomena, we have used structural information obtained from the model NP shapes that best represent our samples (see Table 1). Fig. 5(a) summarizes the evolution of the absolute energy of the absorption peak with increasing measurement temperature for several of our samples. The decrease in the energy shift observed for the small NPs (*e.g.* S1, S2, S4) with increasing annealing temperature is at least partially assigned to the loss of H$_2$. The difference in the energy of the Pt-L_3 XANES absorption peak of our Pt NPs at RT with respect to the measurement at 648 K (lowest H coverage) *versus* N_s/N_t (relative number of atoms at the NP surface) is shown in Fig. 5(b). The highest relative energy shifts were obtained for the NPs with the largest number of low-coordinated surface atoms (S1, S2). A similar result is obtained when the integrated
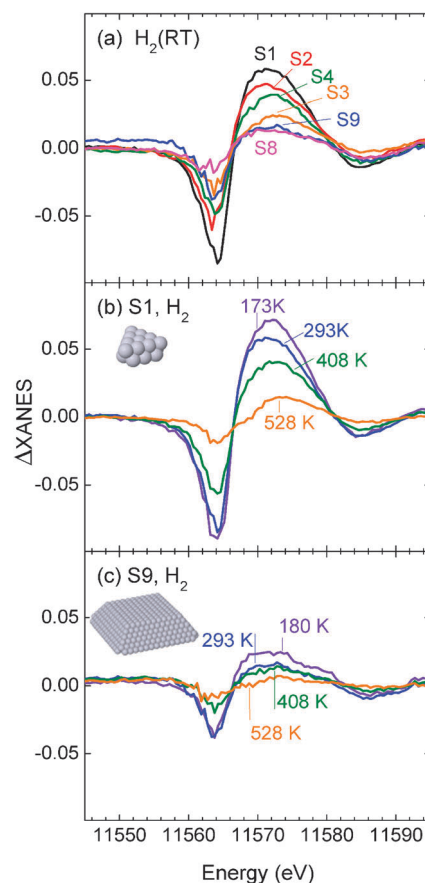
Fig. 4 Difference XANES spectra (ΔXANES) from the Pt-L_3 absorption edge of Pt NPs on γ-Al$_2$O$_3$ displayed as a function of the NP size (a), and the measurement temperature for NPs in S1 (b) and S9 (c). All measurements were conducted in an H$_2$ environment. In all plots, the 648 K data are subtracted from those acquired at lower temperatures (RT in (a) and variable temperatures in (b) and (c)) in order to deconvolute the adsorbate effect, since no significant H$_2$ effect is expected at 648 K.

ΔXANES peak B area is considered, Fig. 6(b). Analogous ΔXANES data comparing low-temperature (166 K–188 K) spectra and 648 K spectra measured in H$_2$ are included in Fig. S4 (ESI†). As was mentioned before, the energy shifts observed at 648 K for the NP samples with respect to bulk Pt might be considered nearly independent of adsorbate effects (lowest effective residual hydrogen coverage due to the low sticking coefficient of hydrogen at this temperature), allowing us to de-couple two extrinsic environmental factors, adsorbate and support effects. When the high temperature energy shifts (with respect to the Pt foil) are plotted *versus* the relative number of atoms within our NPs in contact with the support (N_c/N_t), Fig. 5(c), a linear correlation is observed, with the largest shifts being associated to the samples with 2D shapes, *e.g.*, those with the largest interfacial areas (S1, S4).

To extract additional information on the adsorbate (hydrogen) effect, the evolution of the ΔXANES area of our Pt NP samples with increasing annealing temperature is shown in Fig. 6(a). The peak areas displayed here correspond to the feature labeled "peak B" in the inset of Fig. 6(a). A linear trend was observed for all samples, with decreasing area with

This journal is © the Owner Societies 2012

Phys. Chem. Chem. Phys., 2012, **14**, 11766–11779 | 11771

Fig. 5 (a) Temperature dependence of the absorption peak energy (Pt-L$_3$) of a selected set of Pt NPs on γ-Al$_2$O$_3$ samples: S1, S2, S4–S8. All samples were measured in H$_2$ after reduction. (b) Shift in the Pt-L$_3$ absorption peak energy of NPs with different sizes measured in H$_2$ at RT with respect to data from the same samples acquired at 648 K plotted *versus* the relative number of surface atoms in each NP (N_s/N_t). A Pt foil has been used as reference. (c) Energy shift of the Pt-L$_3$ absorption edge of Pt NPs measured at 648 K with respect to bulk Pt (RT) *versus* the relative number of atoms within the NPs in contact with the NP support (N_c/N_t). All samples were measured in H$_2$ after NP reduction.

increasing temperature, *i.e.*, with decreasing H coverage. In addition, a size-dependent trend was also observed, since different slopes were obtained for NPs with different average size, with the largest slopes corresponding to the smallest NPs (S1, S2). An analogous linear trend was observed when the former areas were normalized by the relative number of atoms at the NP surface (N_s/N_t). Fig. 6(b) displays the former peak B area of samples S1–S5 normalized by N_s/N_t and by the peak B area of S6 (largest NPs available with well-defined shape) measured at 183 K to ensure the maximum initial H$_2$ coverage. After the former normalization, (carried out only for the narrowly size distributed NPs with well-defined average shape) the data sets corresponding to samples of different geometry do not overlap. For example, even at the lowest measurement

temperature, when complete saturation of the NP surface with hydrogen is expected, three different normalized areas corresponding to three different maximum hydrogen saturation coverages were obtained. The different maximum hydrogen saturation coverages are associated to samples with different total number of atoms according to our model shapes, with the largest NPs shown (S5 with 85 atoms and S6 with 140 atoms) having the lowest maximum H coverage (*i.e.*, 1 H per surface Pt atom for S5). The same size-dependent trend is observed at higher temperatures, when partial H desorption sets in. Our normalized data suggest up to about 3 times higher H per Pt ratios for the smallest NPs investigated (S1 and S2) as compared to the larger clusters (S5 and S6). Furthermore, if the area of peak B in ΔXANES plots comparing RT to 648 K H$_2$ data is plotted *versus* N_s/N_t or *versus* the normalized number of broken bonds at the NP surface [12-(total number of Pt–Pt bonds/total number of Pt atoms)], Fig. 6(c) and (d), respectively, a progressive increase in the area is observed with increasing number of surface atoms and with decreasing coordination of the atoms at the NP surface (or increasing number of broken bonds). Since by subtracting data from the same NPs in H$_2$ at high temperature from low or RT data we can gain insight into the role of the adsorbate, the findings in Fig. 6 unveil a direct correlation not only between the maximum hydrogen coverage and the number of atoms at the NP surface, Fig. 6(a), but also that samples with specific shapes characterized by low average atomic coordination at the surface, *i.e.* with a larger fraction of broken bonds, are able to stabilize higher hydrogen coverages, Fig. 6(b) and (d). These results are in agreement with previous theoretical calculations and will be discussed in more detail below.[12,50,51]

(b) Electronic properties (DFT)

The DFT calculations focus on the effects of hydrogen chemisorption on unsupported Pt NPs, with some discussion also of bare NPs. Thus, it is acknowledged that these calculations do not take into account the effect of the support. Since the experimental γ-Al$_2$O$_3$ support has a complex nature (*e.g.* surface hydroxyl groups and related defects[52–55]), including both, the hydrogen and the support effects in our *ab initio* study, which already targets relatively large Pt NPs (up to 85 atoms) is computationally intensive, and outside the scope of this work. Nevertheless, we believe that the theoretical data presented can be used as a guide to provide understanding of the experimental data, especially for the NPs with a 3D-like shape and a small NP/support contact area.

Fig. 7(a) displays calculated d-density of states (d-DOS) of the unsupported, adsorbate-free, Pt NPs with shapes analogous to those extracted from the experimental EXAFS data for Pt$_{22}$, Pt$_{33}$, Pt$_{44}$, Pt$_{55}$, and Pt$_{85}$ (similar to NPs in S1–S5). An interesting conclusion from Fig. 7(a) is that the width of the d-band decreases with decreasing NP size as compared to that of Pt(111) or bulk Pt. This is a result of under-coordination leading to a weaker overlap of the wave functions for the smaller NPs. Nevertheless, for any possible comparison with the XANES data, the center of the *unoccupied* d-DOS band should be considered. For the adsorbate-free model NPs in Fig. 7(a) and bulk reference samples, the unoccupied d-band
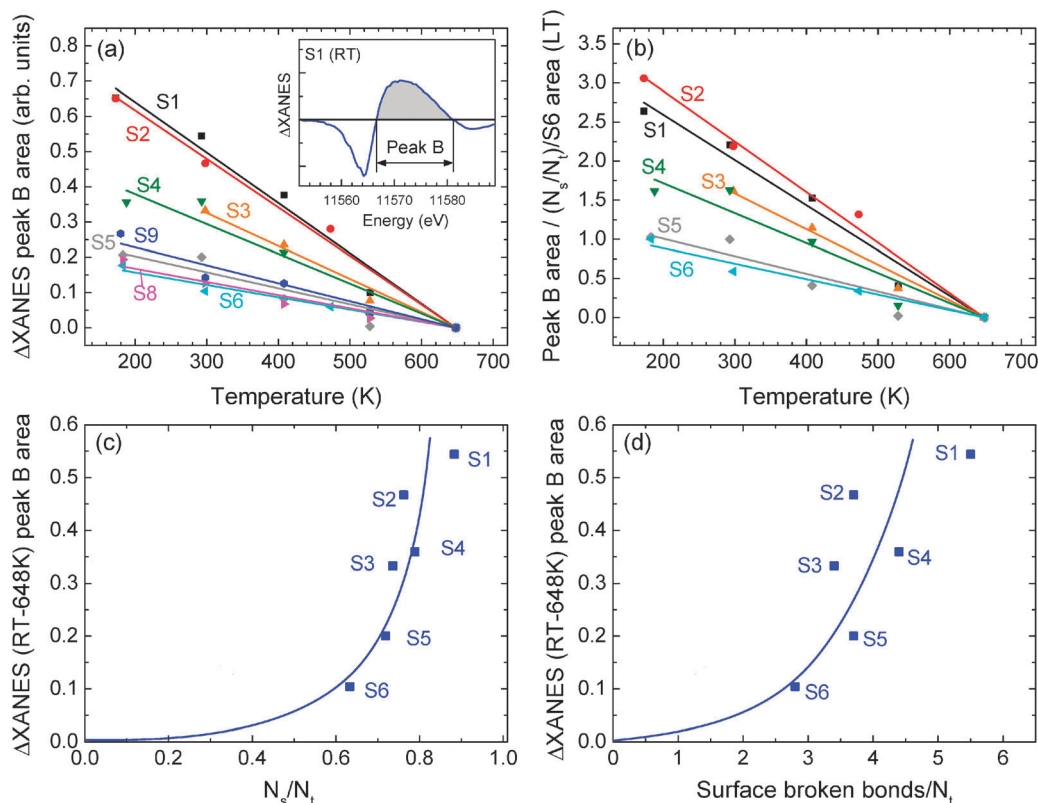
Fig. 6 (a) Evolution of the ΔXANES peak B area (see the inset for definition of peak B) of NPs with different sizes as a function of temperature. All samples were measured in H_2 after NP reduction, (b) the area of the ΔXANES peak B normalized by N_s/N_t and by the area of peak B of S6 measured at 183 K (1H for each surface Pt atom is considered for larger NPs). The N_s/N_t normalization compensates for the fact that larger NPs have a lower number of atoms at their surface affected by H adsorption. ΔXANES (RT – 648 K) peak B area *versus* (c) the relative number of atoms at the NP surface (N_s/N_t), and (d) the relative number of broken bonds at the NP surface (broken/N_t). The broken bonds reflect the presence of Pt atoms at the NP surface with coordination less than 12. The inset in (a) displays a typical ΔXANES spectrum and the shaded area corresponds to peak B.
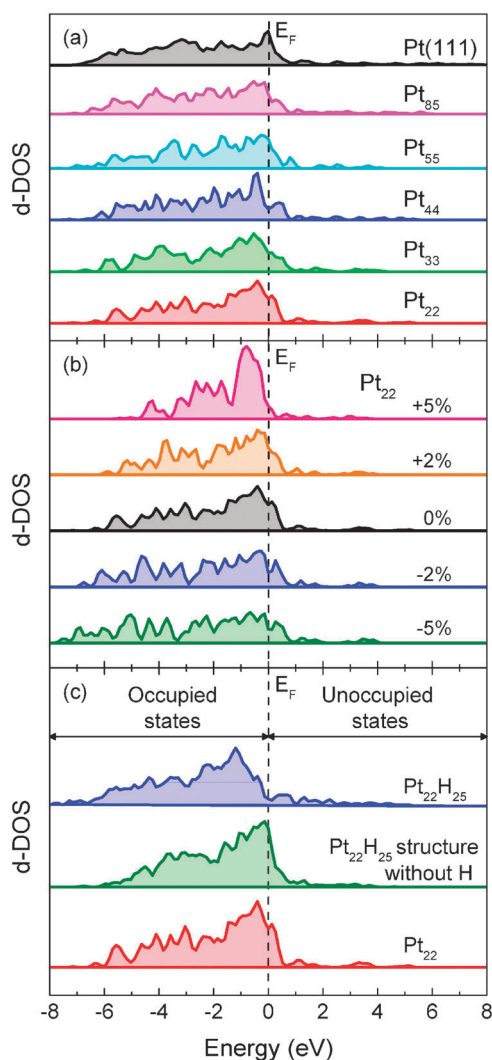
centers are: 1.17 eV (bulk Pt, not shown), 1.22 eV [Pt(111)], 1.14 eV (Pt_{85}), 1.09 eV (Pt_{55}), 1.02 eV (Pt_{44}), 1.02 eV (Pt_{33}), and 0.96 eV (Pt_{22}). The red energy shift obtained with decreasing NP size for the adsorbate-free model Pt NPs is in clear contrast with the trend observed experimentally for the energy of the Pt-L_3 absorption peak maximum in the XANES spectra acquired at 648 K (nearly adsorbate-free), Fig. 5(a). In fact, a size-dependent blue shift was observed in our experiments at all measurement temperatures. This discrepancy might be ascribed to the fact that while the experimental NPs are supported on γ-Al_2O_3, the theoretical NPs are free-standing clusters. Further details will be given in the Discussion section.

No drastic changes in the morphology of the NPs were observed upon hydrogen chemisorption, as demonstrated in Fig. S5 (ESI†), comparing DFT models of Pt_{22}, $Pt_{22}H_{25}$ and $Pt_{22}H_{31}$. Nevertheless, since H chemisorption on Pt NPs induces the relaxation of Pt–Pt distances close to bulk-like bond lengths,[30,38] we have also monitored the evolution of the d-DOS of the unsupported, adsorbate-free, Pt NPs as a function of tensile (similar to the effect induced by adsorbates like H_2) or compressive strain, Fig. 7(b). Tensile strain (+2% and +5%) resulted in a shift of the occupied d-band center away from the Fermi level, while the opposite trend was observed on compressively strained NPs (−2% and −5%). An increase (decrease) in the area of the first peak of the

occupied DOS near E_F was also observed under tensile (compressive) strain. In addition to inducing an expansion of the Pt NP lattice (morphological change), hydrogen adsorption may also modify the electronic structure of the NPs. To deconvolute these two effects, the d-DOS of hydrogen-covered Pt NPs ($Pt_{22}H_{25}$) was compared to that of hydrogen free NPs (Pt_{22}), and that of the $Pt_{22}H_{25}$ geometric structure but without the hydrogen atoms, Fig. 7(c). While the d-DOS of $Pt_{22}H_{25}$ reflects the modifications in the electronic as well as morphological (lattice expansion) structure of the NP induced by hydrogen, the calculations from $Pt_{22}H_{25}$ after hydrogen removal only reflect the influence of lattice relaxations on the d-DOS. As can be seen in Fig. 7(c), the d-DOS of the hydrogen-free NP with the $Pt_{22}H_{25}$ structure is very similar to that of the adsorbate-free Pt_{22}. Therefore, it can be concluded that the changes brought about by hydrogen chemisorption are mainly of electronic nature.

Furthermore, in agreement with previous findings,[17,50,56] addition of hydrogen to our model NPs was found to lead to an increased bandwidth and a shift of both the occupied and the unoccupied d-band centers away from the E_F, Fig. 7(c), 8, 9(a) and (b). Fig. 8 shows the d-DOS of clean Pt_{22} and Pt_{44} together with calculations of Pt_xH_y structures with different hydrogen coverages. The unoccupied d-band center shown in Fig. 9(a) represents the average position of

This journal is © the Owner Societies 2012

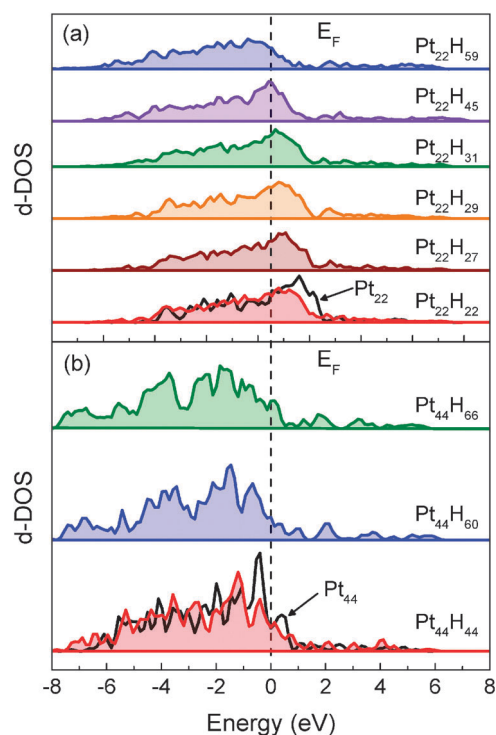*Phys. Chem. Chem. Phys.*, 2012, **14**, 11766–11779 | 11773

Fig. 7 (a) DFT calculated d-electron density of states (d-DOS) of unsupported clean Pt_x NPs (x = 22, 33, 44, 55, 85) and of a Pt(111) surface. (b) Effect of compressive (−) and tensile (+) strain on the d-DOS of unsupported clean Pt_{22}. (c) Comparison of the d-DOS of clean unsupported Pt_{22} to $Pt_{22}H_{25}$ and the same $Pt_{22}H_{25}$ structure but after removing all hydrogen atoms without further lattice relaxation.

Fig. 8 DFT calculated d electron density of states (d-DOS) of unsupported and H-covered (a) $Pt_{22}H_x$ (x = 22, 27, 29, 31, 45, 59) and (b) $Pt_{44}H_x$ (x = 44, 60, 66).

adsorption energies were calculated: $Pt_{22}H_{18}$ (−0.62 eV), $Pt_{22}H_{59}$ (−0.42 eV), $Pt_{44}H_{44}$ (−0.47 eV), $Pt_{44}H_{66}$ (−0.61 eV). The hydrogen adsorption energy of −0.62 eV (−59.8 kJ mol^{-1}) obtained for the lowest hydrogen coverage on $Pt_{22}H_{18}$ is in excellent agreement with the value of −60 kJ mol^{-1} measured experimentally by Bus and van Bokhoven for hydrogen adsorbed on ∼0.8 nm Pt NPs on Al_2O_3, which was assigned to strongly bonded hydrogen.[21]

4. Discussion

Clear changes in the electronic properties of our Pt NPs as compared to bulk Pt could be experimentally observed *via* XANES, in particular, a positive shift in the peak energy and an increase in the integrated intensity of the absorption peak. The origin of these effects has been the subject of intense debate in the literature.[10,15,18,22,25,27,28,44,57–61] While some references attribute the former effects mainly to the interaction of atoms in the Pt NPs with hydrogen, others also involve the NP support. We suggest that some of this discrepancy is due to the difficulty of separating the different contributions to the XANES spectra in the absence of geometrically well-defined NPs with good crystallinity and narrow size distributions, as well as to the challenge of using a unique synthesis approach to generate small NPs with either 2D or 3D shape on the same support in order to evaluate the role of the NP–support interface. Our micellar synthesis has been proven ideal for the generation of size- and shape-selected metal NPs in the sub-2 nm size regime with tunable shape, being thus suitable for the above investigations and subsequent direct comparison with first principle theories.

unoccupied d-DOS states from 0 to 4 eV, and is expected to correlate with the position (energy) of the XANES absorption peak. As can be seen in Fig. 8(a) and 9(a), increasing the hydrogen coverage results in a blue shift of the unoccupied d-band center, which is in agreement with our experimental observation, Fig. 5(a) (increasing energies of the absorption peak with decreasing measurement temperature in hydrogen, *e.g.* with increasing effective H coverage). In addition, a nearly linear correlation between the position of the unoccupied and occupied d-band centers of $Pt_{22}H_x$ and $Pt_{44}H_x$ was obtained with increasing hydrogen content, Fig. 9(a) and (b), respectively.

Fig. 9(c) shows the adsorption energy of hydrogen on Pt_{22} and Pt_{44} NPs as a function of coverage. With increasing hydrogen coverage, the adsorption energy was found to decrease due to adsorbate–adsorbate interactions. For the lowest and highest hydrogen coverages considered, the following
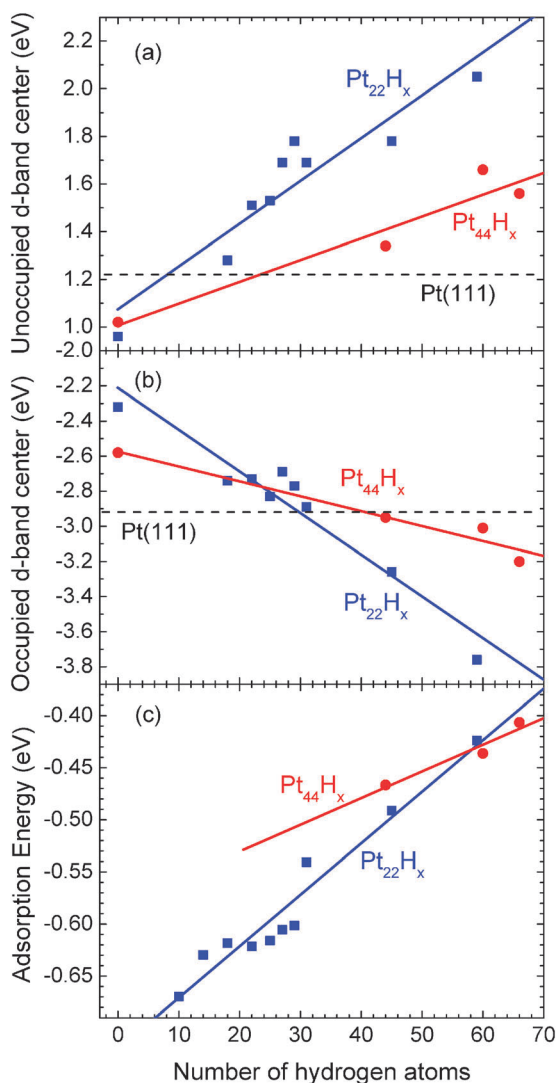
11774 | *Phys. Chem. Chem. Phys.*, 2012, **14**, 11766–11779

This journal is © the Owner Societies 2012

Fig. 9 Center of the d-band of (a) unoccupied and (b) occupied states of unsupported $Pt_{22}H_x$ and $Pt_{44}H_x$ as a function of the number of hydrogen atoms. (c) Adsorption energy of H atoms on Pt_{22} and Pt_{44} as a function of the H coverage.

(a) Adsorbate effects

Strong correlations are expected for size- and adsorbate-effects, since with decreasing NP size there is an increase in the number of surface atoms available for hydrogen chemisorption. Temperature-dependent XANES data can be used to decouple these effects, as for a given NP size, high temperature data (*e.g.* our 648 K data) are expected to be only minimally influenced by adsorbate effects due to the much lower onset temperature for hydrogen desorption.[38] It should be noted that under our experimental conditions (1 atm, 50% H_2 + 50% He) the presence of trace amounts of hydrogen at 648 K cannot be completely ruled out. However, as can be seen in Fig. 5(a), the position of the XANES peak of the small NPs does not change above 528 K, suggesting that the possible residual hydrogen coverage on the NP surface (if any) has already reached its minimum value at that temperature, which is below the 648 K used in our study as reference for the adsorbate-free state of the NPs.

As illustrated in Fig. 3, positive energy shifts as well as an increase in the total integrated XANES peak area beyond the edge were observed with decreasing NP size (TEM diameter) or decreasing 1st NN coordination number (EXAFS). Moreover, there is a correlation between the relative energy shift of the XANES peak at RT (as well as at 173–188 K for H-saturated NPs, see Fig. S4(a), ESI†) with respect to 648 K and the number of atoms at the NP surface (N_s/N_t), Fig. 5(b). The latter finding illustrates that at least part of the energy shift and peak area enhancement are not intrinsic to the specific NP sizes, but due to the chemisorption of hydrogen. This aspect is corroborated based on the comparison of S2 measured in He and H_2 at 173 K, Fig. 1(d). Since S2 is characterized by 3D NPs with a large number of surface atoms (N_s/N_t = 0.84), it constitutes a good example of a NP geometry where adsorbate effects are expected to be dominant. A much smaller spectral area and nearly no energy shift ($\Delta E \sim 0.1$ eV, within our error margin) were observed in He, while an energy shift of +1.0 eV with respect to bulk Pt was measured under H_2, emphasizing the extrinsic nature of the effect observed. Our data thus reveal that the H_2 effect dominates the trends observed.

Regarding the hydrogen effect on Pt NPs and XANES, since H is known to relax the Pt–Pt lattice, the effect can be thought of consisting of two parts: (i) geometrical relaxations of Pt NPs induced by H_2, and (ii) electronic structure changes caused by the formation of H–Pt bonds. Both these effects may lead to energy shifts of the XANES absorption features. Our DFT calculations of the effect of tensile strain on the electronic structure of unsupported *clean* Pt NPs, Fig. 7(b), help us separate these two effects. The effect of tensile strain (an expansion of Pt–Pt bond length) on the d-DOS of Pt_{22} is characterized by a shift in the occupied d-DOS center away from E_F and a suppression of the unoccupied portion near E_F, in analogy with the results obtained for $Pt_{22}H_x$. However, when electronic and geometric effects in the d-DOS of the hydrogen-covered NPs are deconvoluted, Fig. 7(c), the density of states of the $Pt_{22}H_x$ NPs without H (middle panel in Fig. 7(c)) is strikingly similar to that of the clean Pt_{22} (bottom panel in Fig. 7(c)), indicating that the effect of H_2 cannot be simplified as an expansion of the Pt–Pt lattice (intrinsic effect), but it is rather of electronic nature (extrinsic effect). Thus, our DFT results show that the *electronic effect* of hydrogen may be the dominant factor responsible for the modifications of the d-DOS, and possibly for the energy shift in the XANES spectra. An example of the striking effect of hydrogen on small Pt NPs is the reversal of the red shift of the center of the *unoccupied* d-band to a blue shift upon hydrogen adsorption. In particular, while our calculated unoccupied d-band center for *bare* Pt_{22} exhibits a slightly smaller (red) shift with respect to that of Pt_{44} (0.96 eV *vs.* 1.02 eV), upon H_2 adsorption, $Pt_{22}H_{45}$ exhibits not only a blue shift, but also a larger blue shift than that of the larger $Pt_{44}H_{44}$ NPs (1.78 *vs.* 1.34 eV). The latter result is in agreement with the observed relative energy shift of the XANES absorption peaks of S1 and S2, Fig. 3(a). This is also true when the same relative hydrogen coverages are compared: $Pt_{22}H_{22}$ (1.51 eV) *vs.* $Pt_{44}H_{44}$ (1.34 eV).

Theoretically, the increased peak area and positive energy shift described above for the small Pt NPs in hydrogen reflect a

This journal is © the Owner Societies 2012

Phys. Chem. Chem. Phys., 2012, **14**, 11766–11779 | 11775

decrease in the density of electronic states near the Fermi level, *e.g.* the transfer of charge from the NPs to either the support,[20,57,62–64] to hydrogen for the formation of Pt–H bonds (via the creation of anti-bonding states above E_F),[15,16,22,28] or to both. In agreement with previous studies, the Bader atomic charge analysis of H-covered Pt_xH_y NPs shows that there is a net charge transfer from all Pt atoms within the NPs to all hydrogen atoms of 0.55 ($Pt_{22}H_{22}$) and 1.37 electrons ($Pt_{44}H_{44}$). Thus, the remarkable hydrogen effect on the electronic structure of Pt NPs can be attributed to charge transfer from the Pt NPs to hydrogen. However, not all hydrogen atoms receive electrons from the Pt atoms, but primarily those adsorbed at corner and edge sites. The calculated hydrogen adsorption energy in Fig. 9(c) is larger when a smaller number of adsorbed hydrogen atoms are considered, since fewer low coordination sites are available for the higher hydrogen coverages. By comparing similar hydrogen coverages, *e.g.* $Pt_{22}H_{22}$ and $Pt_{44}H_{44}$ in Fig. 9(c), the hydrogen adsorption energy was found to strongly depend on the NP size, with stronger binding of hydrogen to the smaller NPs. This is assigned to the presence of a larger number of sites with low coordination in the smaller NPs.

Quantitative information on the amount of adsorbed hydrogen on Pt NPs has been extracted from the integrated area of the ΔXANES absorption peak,[15,19,22,23,28,64] and a linear correlation between the peak area and the H/Pt ratio established. Some of the former references reported 1.2 : 1 H per Pt atom.[15,22] In the present work, the evolution of the absorption peak energy and integrated ΔXANES (peak B) area with temperature shows a marked size-effect, Fig. 5(a) and 6(a). For all samples measured in H_2, a progressive decrease in the spectral area was observed with increasing temperature for the small NP sizes (≤ 1 nm), while such effect was found to be much less pronounced for the larger clusters. Charge transfer phenomena should be more prominent at low temperature due to the overlap of metal, adsorbate, and support orbitals. The larger WL intensity observed at low temperature for the small NPs, constitutes an indication of a decrease in the total charge within the NPs, which has been transferred to either the hydrogen adsorbate or the support. As can be seen in Fig. 4, 5(b), 6(a) and (b), the adsorbate effect is dominant. In particular, for the samples measured in H_2, the increase in the measurement temperature is expected to lead to a decrease in the effective H_2 coverage on the NP surface, which in turn results in a decrease in the energy shifts, height of the absorption peak WL, and integrated area. As shown in the Theory section, higher charge transfer is expected from metal to hydrogen for Pt atoms with lower coordination numbers. Also, a larger amount of charge transfer should affect the XANES region by inducing larger energy shifts and broadening. Therefore, the smaller NPs would be more affected by hydrogen adsorbates due to: (i) their higher surface/bulk ratio, (ii) larger number of H adsorbate atoms per surface Pt atom, and (iii) larger amount of charge transfer between each H and Pt atom.

Additional information on the role of the NP geometry (size and shape) in the binding of hydrogen can be extracted from Fig. 6(c) and (d). The correlation observed between the number of surface atoms and the ΔXANES peak B area

comparing H-covered NPs (RT data) to nearly adsorbate-free NPs (648 K) of different structures, Fig. 6(c), reveals higher hydrogen coverages at RT on the NPs with the highest number of surface atoms (N_s/N_t). The same trend was observed at all investigated temperatures, including 165–175 K, where the complete saturation of the NP surface with hydrogen is expected. After the normalization of the integrated peak areas by the relative number of surface atoms in each sample and the peak B area of the largest NPs investigated with well-defined geometry (S6), Fig. 6(b), clear size-dependent differences can be seen. In particular, the maximum H coverage stable on the NPs at any given temperature was found to be strongly dependent on the NP geometry. Our data also suggest that the 1 H per 1 Pt atom normalization factor based on H saturation coverages on Pt(111) surfaces, commonly used to describe dispersion in NP samples,[19] cannot be reliably considered to extract quantitative information of the absolute hydrogen coverage per surface atom within small NPs. Indeed, up to 3 H atoms per Pt atom at the NP surface were obtained at the lowest investigated temperatures (166–188 K, Fig. 6(b)). Previous groups reported saturation of the NP surface with 1.2 : 1 H/Pt ratios at room temperature,[15,23] and others used the integrated ΔXANES area at RT in He as a normalization factor in the calculation of relative fractional hydrogen coverages at higher temperatures.[19] Nevertheless, our data indicate that higher H saturation coverages might be obtained at and below RT, and that the 1 : 1 H/Pt ratio commonly used in Langmuir adsorption measurements[65] likely underestimates the amount of H that can be stabilized on the surface of a small Pt NP (≤ 1 nm) with a large fraction of low-coordinated sites (*e.g.* steps, corners and edges). This observation is in agreement with experimental data from Bus *et al.*[21] reporting H/Pt ratios higher than 1 for Pt NPs and Kip *et al.*[66] for Pt, Rh and Ir NPs on Al_2O_3 and SiO_2 (from RT measurements). It is worth mentioning that in the former references the H/Pt ratios were obtained based on the total number of Pt atoms in a NP and not the actual number of surface atoms, as it is considered here. Therefore, even higher H/Pt ratios are expected for the surface atoms. Furthermore, our experimental data also demonstrate that the maximum H saturation coverage is strongly size-dependent, and so is the strength of the Pt–H bond upon sample heating. In addition, the largest ΔXANES areas (*e.g.* largest H coverage) were not only measured for the NP shapes with the highest number of low coordinated surface atoms, Fig. 6(c), but also for those with the largest number of broken bonds at the NP surface, Fig. 6(d). This indicates that more hydrogen atoms can be adsorbed on corner and edge atoms within a NP as compared to higher-coordinated atoms on a Pt(111) surface. Theoretically, H/Pt saturation ratios of up to 4 : 1 have been predicted for small Pt NPs with different structures,[50,51] and higher average hydrogen adsorption energies were obtained for small clusters as compared to bulk. Upon hydrogen saturation, $Pt_{12}H_{30}$ structures were reported on a NaY zeolite[67] based on DFT calculations. Furthermore, a decrease in the hydrogen desorption energy with increasing coverage was observed, reflecting the lower reactivity of the clusters with higher surface hydrogen coverages.[50] A similar trend was observed for our $Pt_{22}H_x$ and $Pt_{44}H_x$ NPs, Fig. 9(a). A size-effect was also described in the literature, with a nearly

linear increase in the number of H atoms chemisorbed on small Pt NPs with increasing NP size (<10 atoms).[17] The same general trend was obtained from our calculations, Fig. 9(c). Simple theoretical models such as the Langmuir model could not reproduce the hydrogen coverage dependence displayed by our experimental system, Fig. 6(a). This is assigned to three important factors: (i) we do not have a single hydrogen desorption site (*e.g.* corners, faces, and edges), and therefore, not a single desorption energy in our complex nanoscale system, (ii) the desorption energy at a given site might be different for NPs of different sizes, (iii) the desorption energy might be coverage dependent, and adsorbate–adsorbate interactions must be considered. These aspects will require future theoretical work and is beyond the scope of the present study.

(b) Support effects

In our experimental work, the relative contribution of the NP support to the electronic properties of our NPs can be inferred from the comparison of samples with identical TEM diameter but different shape (2D *versus* 3D), Fig. 1(a and b). As was described before, larger energy shifts were observed for the flatter NPs, which are the ones with the highest contact area with the support. It should be mentioned that contrary to the case of NPs prepared by conventional impregnation–precipitation synthesis methods, where the final NP geometry is strongly influenced by the nature of the support, our micellar synthesis allows us to create different NP geometries on the same substrate (γ-Al$_2$O$_3$) by changing the metal loading within a given micellar cage. This allows us to compare the electronic properties of 2D and 3D NPs on the same substrate and to separate size from support effects.

Even though with the data at hand we cannot completely exclude the presence of any residual H atoms on the NP surface at 648 K under our experimental conditions, we can still gain insight into the support effect by comparing samples with nearly the same N_s/N_t ratio (same adsorbate effect) but clearly distinct N_c/N_t. For a given NP diameter, the samples with the highest energy shifts (S1 and S4) are also the ones with the highest N_c/N_t ratio (0.55 for S1 and S4 *versus* 0.18–0.23 for S2 and S3), suggesting a correlation between the NP/support contact area and the magnitude of the XANES peak shift and charge transfer or charge redistribution effect. For example, since the N_s/N_t ratios (relative number of surface atoms) for S1 and S2 are nearly identical (0.84–0.86), a similar NP–adsorbate interaction is expected, and the energy shift difference observed while comparing these two samples ($\Delta E \sim 0.5$ eV) must be largely attributed to distinct NP–support interactions. This trend is also illustrated in Fig. 5(c), where the energy shifts measured at high temperature are shown *versus* N_c/N_t. As discussed before, this high temperature data are expected to be the least influenced by adsorbate effects.

As was mentioned in the previous section, contrary trends in the position of the unoccupied d-band center (DFT) and absorption edge peak (high temperature XANES data) were observed with decreasing number of atoms within the NPs for clean unsupported (DFT) and clean (minimum residual H coverage at 648 K) Al$_2$O$_3$-supported (experimental) NPs.

More specifically, red energy shifts were obtained for the model clean NPs with decreasing NP size *via* DFT, while blue shifts were observed for the (nearly hydrogen-free) experimental samples at the highest measurement temperature (648 K). However, it should be noticed that once the hydrogen effect is taken into account, which is mostly an electronic effect *via* charge transfer from Pt atoms to hydrogen, DFT also reproduces blue shifts of the d-band center of H-covered NPs. Provided that a support such as Al$_2$O$_3$ may induce a charge transfer similar to that induced upon hydrogen adsorption (from the Pt NP to Al$_2$O$_3$), the discrepancy between the DFT and the observed experiment mentioned above could be assigned to the support effect, which is not considered in our DFT calculations. This postulation suggests that the experimental trends are not intrinsic to the specific NP geometries, but strongly influenced by environmental effects, in the latter case, by support effects. Following this hypothesis, larger blue shifts would be expected for NPs with a larger fraction of atoms in contact with the support. The correlation between the Pt-L$_3$ peak energy shift of our samples with respect to bulk Pt at 648K and N_c/N_t (contact area with the support) is demonstrated in Fig. 5(c).

In the literature, electronic effects underlying metal–support interactions have been described based on different models. For example, for Pt NPs supported on the LTL zeolite and on SiO$_2$, no net charge transfer was reported.[42,43,64] Instead, modification of the valence orbitals of the metal by the Madelung potential of the support had to be considered.[42,43,64] On the other hand, the transfer of charge from interfacial Pt atoms to defects in Al$_2$O$_3$ was proposed in ref. 64 and 68. Furthermore, *ab initio* calculations by Cooper *et al.*[62] for Pt(111) films on α-Al$_2$O$_3$ revealed the transfer of charge from Pt to the support when the surface is O-terminated, and in the opposite direction when it is Al-terminated. Due to the sample pre-treatment used in our study (prolonged annealing in O$_2$), an oxygen-terminated (hydroxyl) Al$_2$O$_3$ surface is expected, and the direction of the charge transfer inferred here based on the XANES data of the 2D NPs (from Pt to Al$_2$O$_3$) is in agreement with the previous calculations for Pt thin films. A broadening of the Pt-L$_3$ WL due to the interaction of small Pt NPs with LTL-zeolite supports was also previously shown.[10] Nevertheless, other groups reported no support effects on the peak area.[22] In our study, the support effect is evident in the extent of the energy shifts (with respect to bulk Pt).

Our experimental and theoretical findings illustrate the crucial role of not just geometrical effects, but also environmental influences such as adsorbates and the NP support in the electronic properties of small Pt NPs. This level of understanding might be leveraged in order to tune related material properties such as catalytic reactivity. By separating the relative contributions of adsorbate, size, shape, and support effects to the electronic properties of supported NP catalysts, insight can be gained into the influence of each of these parameters on a given catalytic process. For instance, support-induced strain leading to shifts in the d-band center of the supported metals will result in distinct binding of adsorbates to the supported NPs. This might in turn lead to a different catalytic activity, selectivity and stability. Tuning the NP shape might also serve to enhance the NP–support contact

This journal is © the Owner Societies 2012

Phys. Chem. Chem. Phys., 2012, **14**, 11766–11779 | 11777

area, maximizing thus the desired interfacial strain. Another example is the possibility of modifying catalytic performance *via* the selection of NP shapes with distinct crystalline facets and number of low-coordinated surface atoms, which will lead to different adsorbate binding energies and maximum adsorbate coverages. Such geometrical changes have associated specific electronic signatures which can be probed *via* the combination of XANES and DFT methods, provided that the experimental system at hand is geometrically well-defined.

Conclusions

A synergistic combination of XANES, NP shape modeling, and DFT calculations has allowed us to gain insight into the correlations between the structure (size and shape), environment (adsorbate and support) and the electronic properties of unsupported (DFT) and γ-Al_2O_3-supported Pt NPs (XANES). Our data reveal that the size-dependent trends observed in the electronic properties of Pt NPs are not exclusively intrinsic due to the specific NP geometry, but largely due to extrinsic parameters such as the chemisorption of H_2 and NP–support interactions, which are strongly affected by the NP shape and NP–support contact area.

Acknowledgements

References

1 M. Valden, X. Lai and D. W. Goodman, *Science*, 1998, **281**, 1647.
2 A. Naitabdi, L. K. Ono and B. Roldan Cuenya, *Appl. Phys. Lett.*, 2006, **89**, 043101.
3 Q. S. Mei and K. Lu, *Prog. Mater. Sci.*, 2007, **52**, 1175.
4 G. D. Barrera, J. A. O. Bruno, T. H. K. Barron and N. L. Allan, *J. Phys.: Condens. Matter*, 2005, **17**, R217.
5 J. H. Kang, L. D. Menard, R. G. Nuzzo and A. I. Frenkel, *J. Am. Chem. Soc.*, 2006, **128**, 12068.
6 S. I. Sanchez, L. D. Menard, A. Bram, J. H. Kang, M. W. Small, R. G. Nuzzo and A. I. Frenkel, *J. Am. Chem. Soc.*, 2009, **131**, 7040.
7 T. Comaschi, A. Balerna and S. Mobilio, *Phys. Rev. B*, 2008, **77**, 075432.
8 X. Lai, T. P. St Clair, M. Valden and D. W. Goodman, *Prog. Surf. Sci.*, 1998, **59**, 25.
9 D. Bazin, D. Sayers, J. J. Rehr and C. Mottet, *J. Phys. Chem. B*, 1997, **101**, 5332.
10 A. L. Ankudinov, J. J. Rehr, J. J. Low and S. R. Bare, *J. Chem. Phys.*, 2002, **116**, 1911.
11 F. Vila, J. J. Rehr, J. Kas, R. G. Nuzzo and A. I. Frenkel, *Phys. Rev. B*, 2008, **78**, 121404.
12 J. Zhou, X. Zhou, X. Sun, R. Li, M. Murphy, Z. Ding, X. Sun and T.-K. Sham, *Chem. Phys. Lett.*, 2007, **437**, 229.
13 M. W. Tew, J. T. Miller and J. A. van Bokhoven, *J. Phys. Chem. C*, 2009, **113**, 15140.
14 D. E. Ramaker, B. L. Mojet, M. T. Garriga Oostenbrink, J. T. Miller and D. C. Koningsberger, *Phys. Chem. Chem. Phys.*, 1999, **1**, 2293.
15 K. Asakura, T. Kubota, W. J. Chun, Y. Iwasawa, K. Ohtani and T. Fujikawa, *J. Synchrotron Radiat.*, 1999, **6**, 439.
16 Y. Lei, J. Jelic, L. C. Nitsche, R. Meyer and J. Miller, *Top. Catal.*, 2011, **54**, 334.
17 C. G. Zhou, J. P. Wu, A. H. Nie, R. C. Forrey, A. Tachibana and H. S. Cheng, *J. Phys. Chem. C*, 2007, **111**, 12773.
18 A. L. Ankudinov, J. J. Rehr, J. J. Low and S. R. Bare, *J. Synchrotron Radiat.*, 2001, **8**, 578.
19 N. Guo, B. R. Fingland, W. D. Williams, V. F. Kispersky, J. Jelic, W. N. Delgass, F. H. Ribeiro, R. J. Meyer and J. T. Miller, *Phys. Chem. Chem. Phys.*, 2010, **12**, 5678.
20 D. E. Ramaker and D. C. Koningsberger, *Phys. Chem. Chem. Phys.*, 2010, **12**, 5514.
21 E. Bus and J. A. van Bokhoven, *Phys. Chem. Chem. Phys.*, 2007, **9**, 2894.
22 T. Kubota, K. Asakura, N. Ichikuni and Y. Iwasawa, *Chem. Phys. Lett.*, 1996, **256**, 445.
23 S. N. Reifsnyder, M. M. Otten, D. E. Sayers and H. H. Lamb, *J. Phys. Chem. B*, 1997, **101**, 4972.
24 J. A. van Bokhoven and J. T. Miller, *J. Phys. Chem. C*, 2007, **111**, 9245.
25 N. Ichikuni and Y. Iwasawa, *Catal. Lett.*, 1993, **20**, 87.
26 A. L. Ankudinov, J. J. Rehr, J. J. Low and S. R. Bare, *Top. Catal.*, 2002, **18**, 3.
27 M. K. Oudenhuijzen, J. A. van Bokhoven, J. T. Miller, D. E. Ramaker and D. C. Koningsberger, *J. Am. Chem. Soc.*, 2005, **127**, 1530.
28 T. Kubota, K. Asakura and Y. Iwasawa, *Catal. Lett.*, 1997, **46**, 141.
29 N. Schweitzer, H. Xin, E. Nikolla, J. T. Miller and S. Linic, *Top. Catal.*, 2010, **53**, 348.
30 B. Roldan Cuenya, J. R. Croy, S. Mostafa, F. Behafarid, L. Li, Z. Zhang, J. C. Yang, Q. Wang and A. I. Frenkel, *J. Am. Chem. Soc.*, 2010, **132**, 8747.
31 J. R. Croy, S. Mostafa, H. Heinrich and B. Roldan Cuenya, *Catal. Lett.*, 2009, **131**, 21.
32 A. Naitabdi, F. Behafarid and B. Roldan Cuenya, *Appl. Phys. Lett.*, 2009, **94**, 083102.
33 S. Mostafa, F. Behafarid, J. R. Croy, L. K. Ono, L. Li, J. C. Yang, A. I. Frenkel and B. Roldan Cuenya, *J. Am. Chem. Soc.*, 2010, **132**, 15714.
34 L. K. Ono, B. Yuan, H. Heinrich and B. Roldan Cuenya, *J. Phys. Chem. C*, 2010, **114**, 22119.
35 B. Roldan Cuenya, L. K. Ono, J. R. Croy, K. Paredis, A. Kara, H. Heinrich, J. Zhao, E. E. Alp and W. Keune, *Phys. Rev. B*, 2012, submitted.
36 M. S. Nashner, A. I. Frenkel, D. L. Adler, J. R. Shapley and R. G. Nuzzo, *J. Am. Chem. Soc.*, 1997, **119**, 7760.
37 M. S. Nashner, D. M. Somerville, P. D. Lane, D. L. Adler, J. R. Shapley and R. G. Nuzzo, *J. Am. Chem. Soc.*, 1996, **118**, 12964.
38 B. Roldan Cuenya, M. Alcántara Ortigoza, L. Ono, F. Behafarid, S. Mostafa, J. Croy, K. Paredis, G. Shafai, T. Rahman, L. Li, Z. Zhang and J. Yang, *Phys. Rev. B: Condens. Matter Mater. Phys.*, 2011, **84**, 245438.
39 B. Roldan Cuenya, A. I. Frenkel, S. Mostafa, F. Behafarid, J. R. Croy, L. K. Ono and Q. Wang, *Phys. Rev. B*, 2010, **82**, 155450.
40 A. I. Frenkel, C. W. Hills and R. G. Nuzzo, *J. Phys. Chem. B*, 2001, **105**, 12689.
41 R. Prins and D. C. Koningsberger, in *X-ray absorption. Principles, applications, techniques of EXAFS, SEXAFS, and XANES*, ed. D. C. Koningsberger and R. Prins, Wiley, New York, vol. 8, ch. 8, 1988.
42 J. T. Miller, B. L. Mojet, D. E. Ramaker and D. C. Koningsberger, *Catal. Today*, 2000, **62**, 101.
43 B. L. Mojet, J. T. Miller, D. E. Ramaker and D. C. Koningsberger, *J. Catal.*, 1999, **186**, 373.

11778 | *Phys. Chem. Chem. Phys.*, 2012, **14**, 11766–11779

This journal is © the Owner Societies 2012

44 M. Vaarkamp, B. L. Mojet, M. J. Kappers, J. T. Miller and D. C. Koningsberger, *J. Phys. Chem.*, 1995, **99**, 16067.
45 A. N. Mansour, J. W. Cook and D. E. Sayers, *J. Phys. Chem.*, 1984, **88**, 2330.
46 P. Hohenberg and W. Kohn, *Phys. Rev.*, 1964, **136**, B864.
47 G. Kresse and J. Furthmuller, *Phys. Rev. B*, 1996, **54**, 11169.
48 G. Kresse and D. Joubert, *Phys. Rev. B*, 1999, **59**, 1758.
49 J. P. Perdew, K. Burke and M. Ernzerhof, *Phys. Rev. Lett.*, 1996, **77**, 3865.
50 L. Chen, A. C. Cooper, G. P. Pez and H. Cheng, *J. Phys. Chem. C*, 2007, **111**, 5514.
51 A. Vargas, G. Santarossa and A. Baiker, *J. Phys. Chem. C*, 2011, **115**, 10661.
52 M. Delgado, F. Delbecq, C. C. Santini, F. Lefebvre, S. Norsic, P. Putaj, P. Sautet and J. M. Basset, *J. Phys. Chem. C*, 2012, **116**, 834.
53 M. Digne, P. Sautet, P. Raybaud, P. Euzen and H. Toulhoat, *J. Catal.*, 2004, **226**, 54.
54 M. Digne, P. Sautet, P. Raybaud, H. Toulhoat and E. Artacho, *J. Phys. Chem. B*, 2002, **106**, 5155.
55 M. Digne, P. Sautet, P. Raybaud, P. Euzen and H. Toulhoat, *J. Catal.*, 2002, **211**, 1.
56 B. Hammer and J. K. Norskov, *Nature*, 1995, **376**, 238.
57 M. Vaarkamp, J. T. Miller, F. S. Modica, G. S. Lane and D. C. Koningsberger, *Jpn. J. Appl. Phys.*, 1993, **32**(Suppl. 32–2), 454.
58 M. M. Otten, M. J. Clayton and H. H. Lamb, *J. Catal.*, 1994, **149**, 211.
59 M. G. Samant and M. Boudart, *J. Phys. Chem.*, 1991, **95**, 4070.
60 A. V. Soldatov, S. Della longa and A. Bianconi, *Solid State Commun.*, 1993, **85**, 863.
61 T. Matsuura, T. Fujikawa and H. Kuroda, *J. Phys. Soc. Jpn.*, 1983, **52**, 3275.
62 V. R. Cooper, A. M. Kolpak, Y. Yourdshahyan and A. M. Rappe, *Phys. Rev. B*, 2005, **72**, 081409(R).
63 M. Sugimoto, H. Katsuno, T. Hayasaka, N. Ishikawa and K. Hirasawa, *Appl. Catal., A*, 1993, **102**, 167.
64 D. C. Koningsberger, J. de Graaf, B. L. Mojet, D. E. Ramaker and J. T. Miller, *Appl. Catal., A*, 2000, **191**, 205.
65 L. Spenadel and M. Boudart, *J. Phys. Chem.*, 1960, **64**, 204.
66 B. J. Kip, F. B. M. Duivenvoorden, D. C. Koningsberger and R. Prins, *J. Catal.*, 1987, **105**, 26.
67 X. Liu, H. Dilger, R. A. Eichel, J. Kunstmann and E. Roduner, *J. Phys. Chem. B*, 2006, **110**, 2013.
68 J. H. Kwak, J. Hu, D. Mei, C.-W. Yi, D. H. Kim, C. H. F. Peden, L. F. Allard and J. Szanyi, *Science*, 2009, **325**, 1670.